Available online at www.sciencedirect.com
ScienceDirect
Trans. Nonferrous Met. Soc. China 23(2013) 956−963
Transactions of Nonferrous Metals Society of China
www.tnmsc.cn

Effect of initial microstructure on hot workability of 7085 aluminum alloy

Song-yi CHEN, Kang-hua CHEN, Guo-sheng PENG, Le JIA

State Key Laboratory of Powder Metallurgy, Central South University, Changsha 410083, China

Received 9 March 2012; accepted 10 October 2012

Abstract: The hot workability of 7085 aluminum alloys with different initial microstructures (as-homogenized and as-solution treated) was studied by isothermal compression tests at the deformation temperature ranging from 300 to 450 °C and the strain rate ranging from 0.0001 to 1 s^{-1}. The strain rate sensitivity of the alloy was evaluated and used for establishing the power dissipation maps and instability maps on the basis of the flow stress data. The results show that the efficiency of power dissipation for the as-homogenized alloy is lower than that of the as-solution treated alloy. The deformation parameters of the dynamic recrystallization for the as-homogenized and as-solution treated alloy occur at 400 °C, 0.01 s^{-1} and 450 °C, 0.001 s^{-1}, respectively. The flow instability region of the as-homogenized alloy is narrower than that of the as-solution treated alloy. These differences of the alloys with two different initial microstructures on the processing maps are mainly related to the dynamic precipitation characteristics.
Key words: 7085 aluminum alloy; initial microstructure; hot workability; processing map; strain rate sensitivity

1 Introduction

Al−Zn−Mg−Cu alloys have been widely used as structural materials in aerospace due to their low density, excellent stress corrosion resistance and fracture toughness [1,2]. The hot deformation behavior and workability of Al−Zn−Mg−Cu alloys were the crucial parameters to characterize plastic deformation properties. A number of studies have been put forward to understand the hot deformation behavior, which mainly focused on the flow stress curves, constitutive equations and the deformation mechanism. JIN et al [3] investigated the hot deformation behavior of 7150 aluminum alloy and found that the peak flow stress decreased with increasing the deformation temperature and decreasing the strain rate. ZHEN et al [4] demonstrated that the average grain boundary misorientation angle of 7050 aluminum alloy after high temperature compression increased with the increase of deformation temperature. HU et al [5] reported that the main deformation mechanism of 7050 aluminum alloy was grain boundary slip at large Z parameter value while grain boundaries sliding at small Z parameter value. The processing map has been developed and used for optimizing and evaluating the thermal deformation mechanisms of metal materials, such as magnesium alloy [6,7], aluminum alloy [8−10] and titanium alloy [11,12].

The processing map on the basis of the dynamic material model (DMM) was developed by PRASAD et al [13]. According to the model, the work-piece undergoing hot deformation is considered to be a dissipater of power and the total power dissipation (P) might be dissipated into two parts: G and J.

$$P=\sigma\dot{\varepsilon}=G+J=\int_0^{\dot{\varepsilon}}\sigma \mathrm{d}\dot{\varepsilon}+\int_0^{\sigma}\dot{\varepsilon}\mathrm{d}\sigma \tag{1}$$

where G represents the power dissipated by plastic work, J is related to the power dissipation by metallurgical process, such as dynamic recovery, dynamic recrystallization, dissolution or growth of particles, and phase transformation [12,14−16].

The relationship between G and J is related to strain rate sensitive parameter (m), which is given as follows:

$$\frac{\mathrm{d}J}{\mathrm{d}G}=\frac{\sigma \mathrm{d}\dot{\varepsilon}}{\dot{\varepsilon}\mathrm{d}\sigma}=\frac{\mathrm{d}(\ln\sigma)}{\mathrm{d}(\ln\dot{\varepsilon})}=m \tag{2}$$

For an ideal linear dissipating body, m=1 and $J=J_{max}=P/2$. The power dissipation capacity of the alloy can be evaluated by the efficiency of power dissipation

Foundation item: Projects (2010CB731701, 2012CB619502) supported by the National Basic Research Program of China; Project (CX2012B043) supported by Hunan Provincial Innovation Foundation for Postgraduate, China; Project (51021063) supported by Creative Research Group of National Natural Science Foundation of China
Corresponding author: Kang-hua CHEN; Tel: +86-731-88830714; Fax: +86-731-88710855; E-mail: khchen@mail.csu.edu.cn
DOI: 10.1016/S1003-6326(13)62552-2

(η), which is defined as follows [13]:

$$\eta = \frac{J}{J_{\max}} = \frac{2m}{m+1} \tag{3}$$

A continuum instability criterion based on the extreme principles of irreversible thermodynamics is used to identify the regions of flow instabilities. According to the criterion, the flow instability can be expressed as follows:

$$\zeta(\dot{\varepsilon}) = \frac{\partial \ln[m/(m+1)]}{\partial \ln \dot{\varepsilon}} + m < 0 \tag{4}$$

The variation of the instability parameter $\zeta(\dot{\varepsilon})$ with temperature and strain rate can be expressed by the instability maps to delineate instability regions of negative $\zeta(\dot{\varepsilon})$ value.

Moreover, previous investigations showed that the processing maps were significantly influenced by the initial microstructures. ANBU and RAMANATHAN [17] reported that the extruded ZE41A magnesium alloy showed higher efficiency of power dissipation and lower instability regions than the as-cast alloy. VENUGOPAL et al [14] found that the peak efficiency of power dissipation of dynamic recrystallization (DRX) was higher in the as-cast material than that in the wrought AISI 304 stainless steel. RAVICHANDRAN and PRASAD [18] revealed that the peak efficiency of power dissipation domain rotated slightly toward lower strain rates and lower temperature with increasing aluminum purity. LEE et al [11] assessed the hot workability of the as-cast and forged Ti−8Ta−3Nb alloys using processing maps. They concluded that the efficiency of power dissipation of the forged specimens was higher than that of the as-cast specimen. Therefore, it is necessary to understand the initial microstructure on the workability and improve the hot processing of aluminum alloys.

7085 aluminum alloy was developed as the new generation of high strength and thick plate alloy, which has higher fracture toughness and lower quench sensitivity than 7050 aluminum alloy. Although some works have been done for 7085 aluminum alloy [19−21], few studies are related to the hot workability of the alloy with processing map, especially different initial microstructures. In this work, the effect of the initial microstructure (as-homogenized and as-solution treated) on workability of 7085 aluminum alloy was studied through processing maps and microstructure observations.

2 Experimental

The experiments were carried out on 7085 aluminum alloy with main chemical compositions of 7.5% Zn, 1.6% Mg, 1.5% Cu, 0.12% Zr and Al balance (mass fraction, %). The specimens were subjected to homogenization and solution heat treatment. The homogenization treatment was as follows: the as-cast billets were homogenized at 450 °C for 24 h and 470 °C for 30 h, and cooled to room temperature. The solution treatment was as follows: the homogenized billets were forged at 400−450 °C and strain of about 3, and then solution-treated at 470 °C for 1 h, followed by water quenching.

Cylindrical samples with 10 mm in diameter and 15 mm in height were machined from the homogenized billets and solution treated plates. The compression tests were carried out on a Gleeble 1500 at temperatures from 300 to 450 °C and strain rate from 0.0001 s^{-1} to 1 s^{-1}. Before the compression, the specimens were heated to the deformation temperature at a heating rate of 10 °C/s, and then held for 3 min at the deformation temperature. Subsequently, the specimens were compressed to 50% reduction, and quenched in water immediately. In order to reduce the frictional force between the specimens and the press indenters, a graphite lubricant was used during the isothermal compression tests. The microstructures of the deformed specimens were examined by OM and TEM (JEOL−2100F). Thin foils for TEM were prepared by mechanical polishing to 80−100 μm and final twin-jet electro polishing in a solution of 25% HNO_3+75% CH_3OH at −25 °C.

3 Results

3.1 Initial microstructure

The initial microstructures of the two heat-treated alloys are shown in Fig. 1. For the as-homogenized alloy, the grain size is about 100 μm, and some undissolved primary particles distribute along the grain boundaries. The particles are probably undissolved *S* ($A1_2CuMg$) phase (Fig. 1(a)). However, the grain size is about 30 μm and there are few coarse particles on the grain boundaries for the as-solution treated alloy (Fig. 1(b)).

3.2 Flow stress

The flow stress curves of the as-homogenized and as-solution treated alloys at various deformation temperatures and strain rates are shown in Figs. 2 and 3, respectively. The results show that, for the alloys after different treatments, the flow stress increases rapidly with increasing the strain at the initial stage, and then nearly keeps stable or decreases with strain beyond the peak strain. The flow stress decreases with the decrease of strain rate and the increase of deformation temperature. It is clear that the flow stress of the as-solution treated alloy is higher than that of the as-homogenized alloy, especially at low deformation temperature. The detailed description and comparison were shown in Ref. [20].

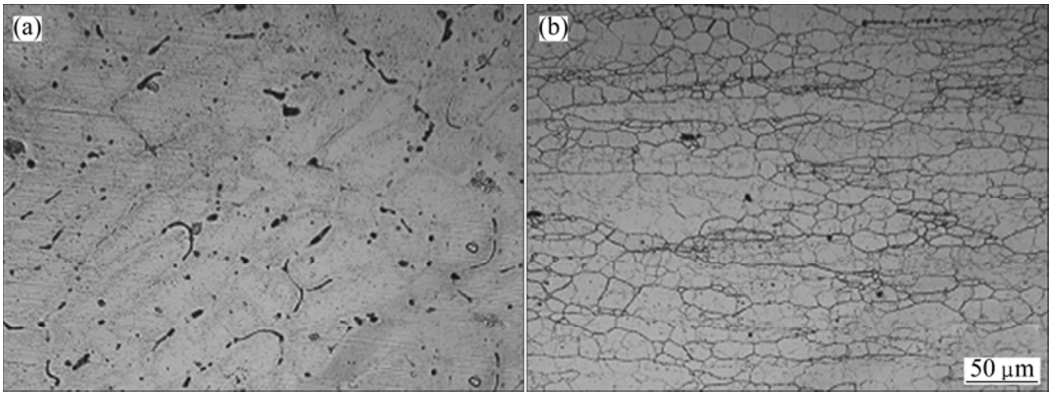

Fig. 1 Initial microstructures of alloys: (a) As-homogenized; (b) As-solution treated

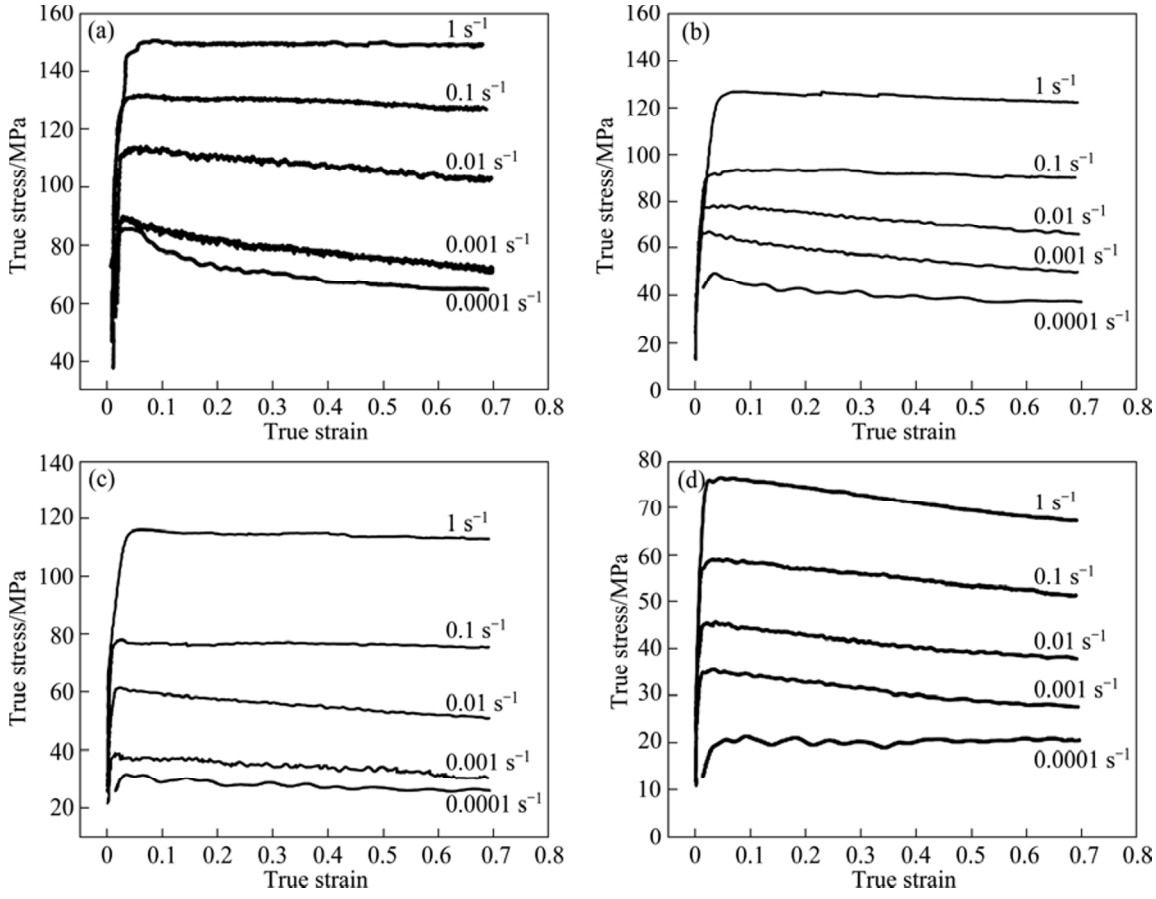

Fig. 2 Flow stress curves of as-homogenized alloys at different deformation temperatures: (a) 300 °C; (b) 350 °C; (c) 400 °C; (d) 450 °C

3.3 Processing map

Figure 4 shows the $\lg\sigma$—$\lg\dot{\varepsilon}$ curves of the alloys at the strain of 0.5 and different temperatures under different initial microstructures. The strain rate sensitivity (m) was evaluated by the three order polynomial fitting of the $\lg\sigma$—$\lg\dot{\varepsilon}$ curves. The efficiency of power dissipation (η) was calculated according to Eq. (3), and the flow instability was calculated based on Eq. (4).

The processing maps for the alloy at the strain of 0.5 under different initial microstructures are shown in Fig. 5. The contour numbers represent the efficiency of power dissipation and the shade area corresponds to the instable region. The processing maps reveal the following characteristics under different initial microstructures.

1) The efficiency of power dissipation of the as-solution treated alloy is higher than that of the as-homogenized alloy.

2) For the as-homogenized alloy, one domain with a higher value of power dissipation is obtained, which is in

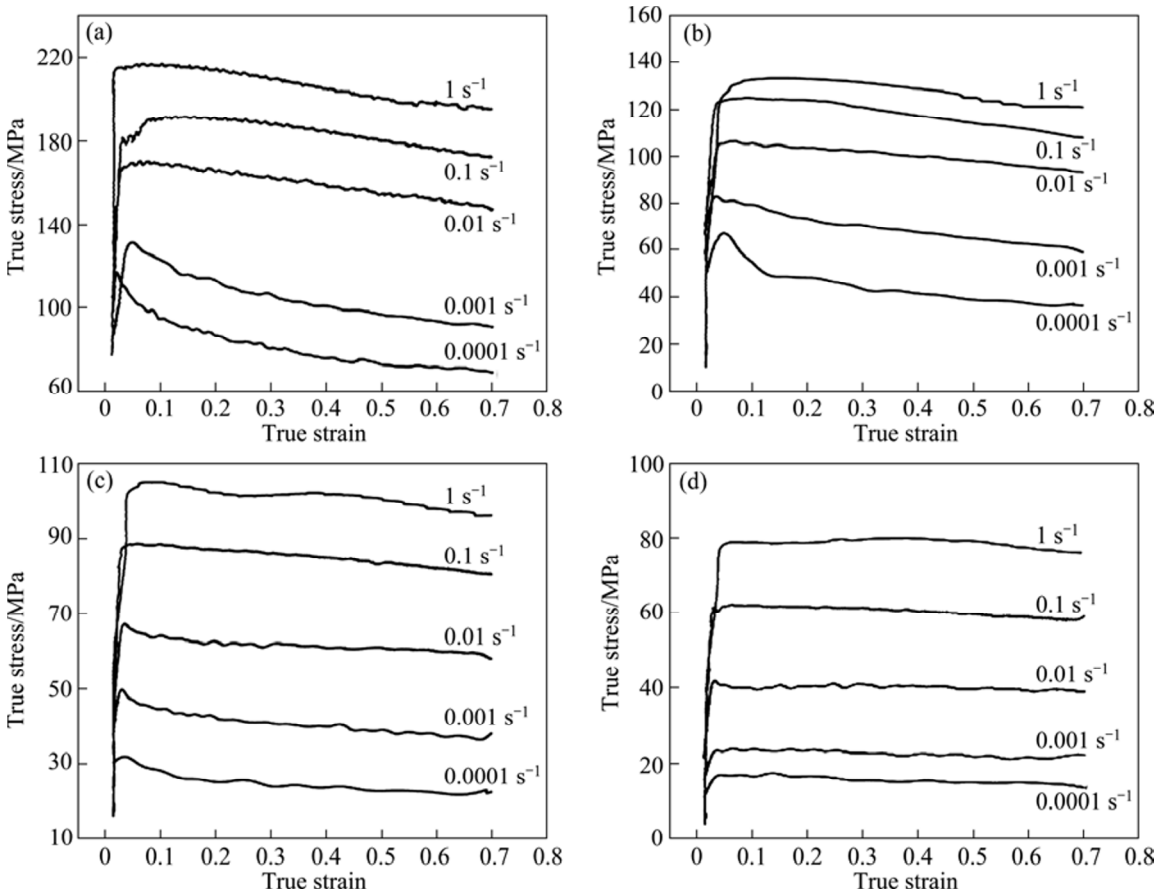

Fig. 3 Flow stress curves of as-solution treated alloys at different deformation temperatures: (a) 300 °C; (b) 350 °C; (c) 400 °C; (d) 450 °C

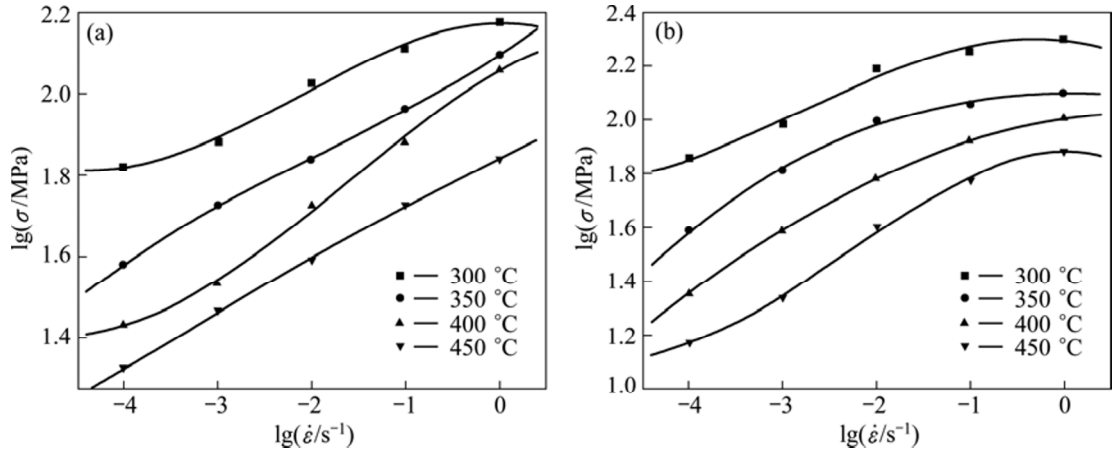

Fig. 4 lg σ—lg $\dot{\varepsilon}$ curves of alloys at strain of 0.5 and different temperatures under different initial microstructures: (a) As-homogenized; (b) As-solution treated

the temperature range of 380−450 °C and strain rate range of 0.001−1 s^{-1} with a peak efficiency of power dissipation of 28% at about 400 °C and 0.01 s^{-1}.

3) For the as-solution treated alloy, two domains with higher value of power dissipation are obtained. One is in the temperature range of 300−400 °C and strain rate range of 0.0001−0.001 s^{-1} with a peak efficiency of power dissipation of 46% at 350 °C and 0.0001 s^{-1}. The other is in the temperature range of 420−450 °C and the strain rate range of 0.001−0.1 s^{-1} with a peak efficiency of power dissipation of about 42% at 450 °C and 0.001 s^{-1}.

4) The instability region is significantly affected by the initial microstructures of the alloys. The flow instability region of the as-solution treated alloy is wider than that of the as-homogenized alloy.

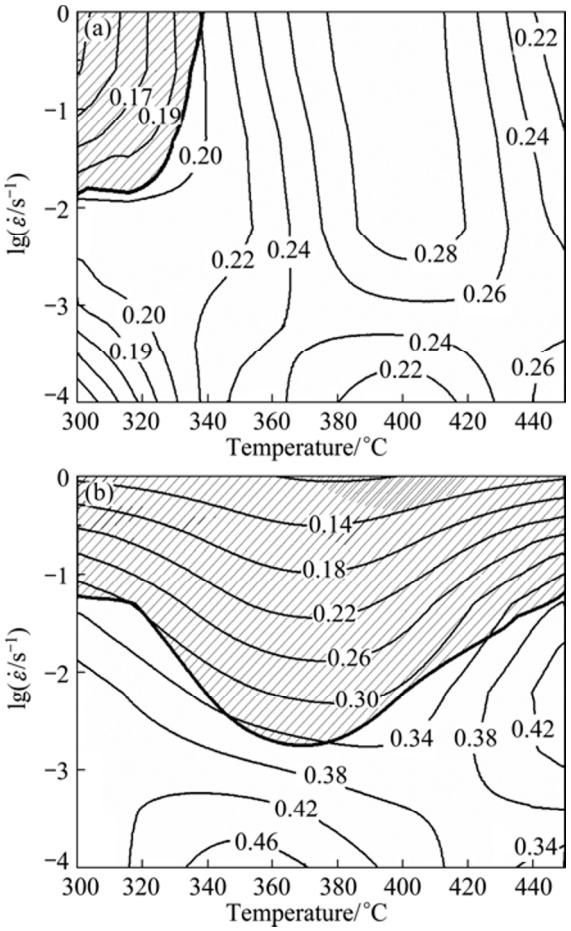

Fig. 5 Processing maps for alloys at strain of 0.5 under different initial microstructures: (a) As-homogenized; (b) As-solution treated

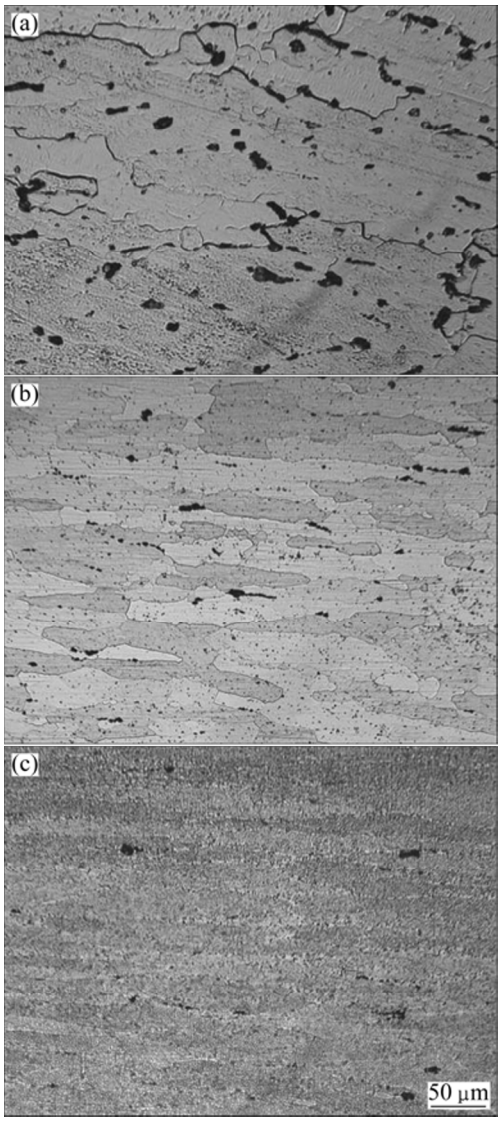

Fig. 6 Optical microstructures of alloys deformed at peak efficiency of power dissipation domain: (a) As-homogenized alloy deformed at 400 °C and 0.01 s^{-1}; (b) As-solution treated alloy deformed at 450 °C and 0.001 s^{-1}; (c) As-solution treated alloy deformed at 350 °C and 0.0001 s^{-1}

4 Discussion

The efficiency of power dissipation during hot working of materials is contributed to several dynamic metallurgical processes, such as dynamic recovery, dynamic recrystallization, and dissolution or growth of particles [14−16]. Therefore, in order to understand the deformation mechanism, it is necessary to consider the interactions of all aspects. Figure 6(a) shows the microstructure of the as-homogenized alloy deformed at 400 °C and 0.01 s^{-1}, which corresponds to the peak efficiency of power dissipation of 28%. It can be seen from Fig. 6(a) that some recrystallized grains exist at the grain boundaries, indicating that the dynamic recrystallization occurs. Therefore, according to the above observation, the peak efficiency of power dissipation for the as-homogenized alloy at 400 °C and 0.01 s^{-1} can be interpreted in terms of the dynamic recrystallization. The efficiency of power dissipation for the as-solution treated alloy is different from that of the as-homogenized alloy. Two domains with higher value of power dissipation are obtained. One domain with a peak efficiency of power dissipation (42%) occurs at 450 °C and 0.001 s^{-1}, and the other domain with a peak efficiency of power dissipation (46%) occurs at 350 °C and 0.0001 s^{-1}. Figure 6(b) shows the typical micrograph of the as-solution treated alloy deformed at 450 °C and 0.001 s^{-1}. It can be seen that some recrystallized grains exist at the grain boundaries, indicating that the dynamic recrystallization occurs. It is also observed that the solution-treated alloy shows the higher volume fraction of recrystallized grains than the homogenized alloy. However, there are no recrystallized grains at the grain boundaries, but there are many fine precipitates for the as-solution treated alloy deformed at 350 °C and 0.0001 s^{-1} (Fig. 6(c)). Figure 7 shows the TEM microstructures

of the as-homogenized alloy deformed at different strain rates and 350 °C. The high density of dislocation tangles with large size of precipitates on the matrix and along grain boundary at the strain rate of 1 s^{-1} (Fig. 7(a)). The dislocation density slightly decreases and the distribution of precipitates does not obviously change at the strain rate of 0.1 s^{-1} (Fig. 7(b)).

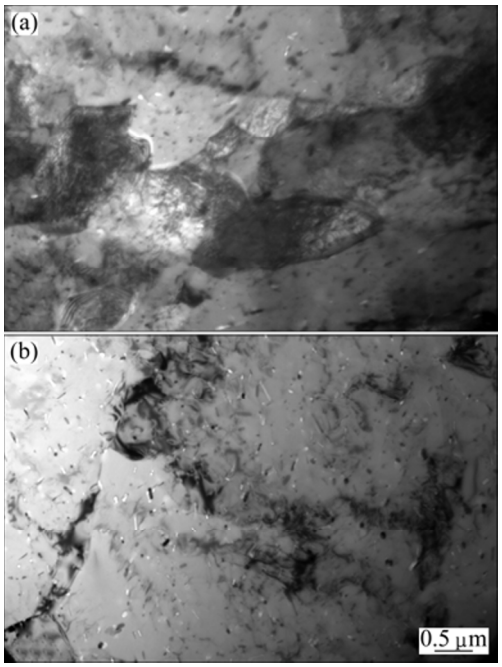

Fig. 7 TEM micrographs of as-homogenized alloys deformed at 350 °C and different strain rates: (a) 1 s^{-1}; (b) 0.1 s^{-1}

Figure 8 shows the typical TEM micrographs of the as-solution treated alloy deformed at different strain rates and 350 °C. Fine precipitates homogenously distribute on the matrix and coarse precipitates appear along grain boundaries at the strain rate of 1 s^{-1}. The number of the precipitates decreases and the size of precipitates increases at the strain rate 0.001 s^{-1}. Therefore, according to the above analyses, the map exhibits a domain of dynamic recrystallization occurring at 450 °C and 0.001 s^{-1} while a domain of dynamic precipitation and coarsening occurs at 350 °C and 0.0001 s^{-1} for the as-solution treated alloy.

Meanwhile, the peak efficiency of power dissipation for the as-solution treated alloy is higher than that of as-homogenized alloy (Fig. 5). One domain of dynamic recrystallization for the as-homogenized and as-solution treated alloys occurs at 400 °C, 0.01 s^{-1} and 450 °C, 0.001 s^{-1}, respectively, and the other domain of dynamic precipitation and particles coarsening occurs at 350 °C and 0.0001 s^{-1} for the as-solution treated alloy. These results can be explained from the following aspects: 1) Dynamic precipitation. The high supersaturation of solid solution of the solution-treated alloy results in dynamic precipitation. Fine precipitates homogenously distribute

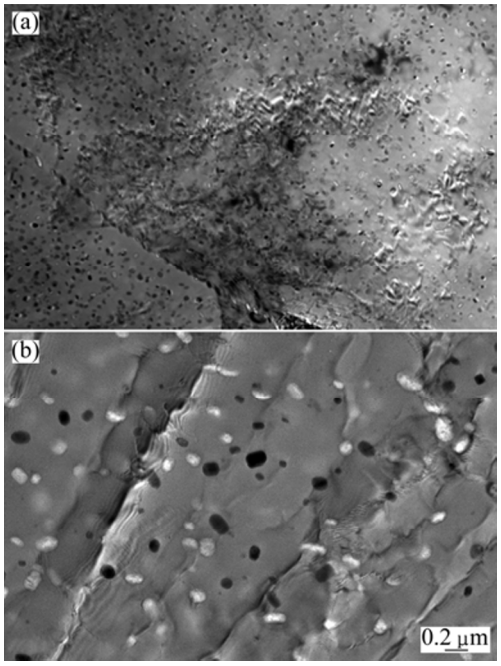

Fig. 8 TEM micrographs of as-solution treated alloy deformed at 350 °C and different strain rates: (a) 1 s^{-1}; (b) 0.001 s^{-1}

on the matrix and coarse precipitates appear along grain boundaries. With decreasing the strain rate, the number of the precipitates decreases and the size of the precipitates increases (Fig. 8). However, low super-saturation of solid solution of the as-homogenized alloy is due to slow cooling after homogenization treatment, few fine precipitates under the deformation. 2) Residual solute remaining in the solid solution. There is much more residual solution remaining in the solution-treated alloy than in the homogenized alloy. The effect will decrease and become negligible as precipitates proceed with increasing the strain, and the stability difference of both conditions will be less effective due to the element removal from matrix faster at high temperatures. 3) The interaction between precipitate and dislocation. The fine precipitates in the as-solution treated alloy interact with the dislocation and inhibit dynamic recrystallization. However, for the as-homogenized alloy, the large constituent phases in the grain can act as the particle stimulated nucleation (PSN) and promote the recrystallization. 4) Grain size. The fine grain size of the solution-treated alloy facilitates the recrystallization, which provides a number of available sites for the recrystallization nucleation.

Compared with the instability region of the as-solution treated alloy and as-homogenized alloy, it is found that the instability region of the as-solution treated alloy is wider than that of the as-homogenized alloy (Fig. 5). These predictions are validated by the microstructural observations on the deformed specimens. Figure 9 shows the microstructure of the as-homogenized

alloy deformed at 300 °C and 1 s^{-1}. Figure 10 shows the microstructure of the as-solution treated alloy deformed at 350 °C and 1 s^{-1}. It can be seen that under the two conditions, the microstructures reveal intense adiabatic shear bands, which can be described as unstable deformation regions corresponding to instability maps. Generally speaking, the flow instability region of the fine grain material can be wider than that of the coarse grains. However, the precipitation characteristics of the alloys cannot be neglected. Less constituent and smaller grain size are characterized for the as-solution treated alloy compared with the as-homogenized alloy, which benefits to the ductility. But a large number of fine precipitates promote work hardening and inhibit the dynamic recovery, and the solute level increases both in the grain and precipitation free zones (PFZ). Thus, the ability for local grain flow to relieve stress is greatly reduced. Consequently, the strong lattice does not accommodate the grain boundary sliding, and enhances the susceptibility to cracking. These phenomena were confirmed by CERRI et al [22]. They found that the as-solution treated 7075 aluminum alloy has lower workability than the as-cast alloy at low deformation temperatures.

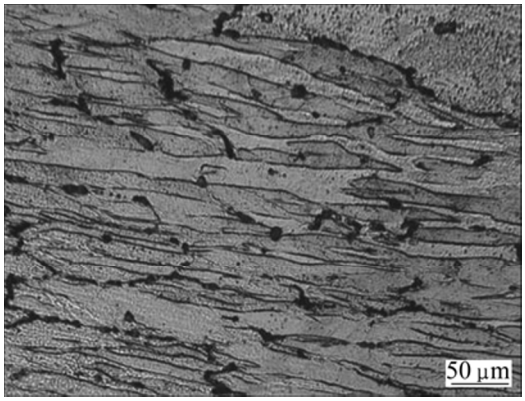

Fig. 9 Microstructure of as-homogenized alloy deformed at 300 °C and 1 s^{-1}

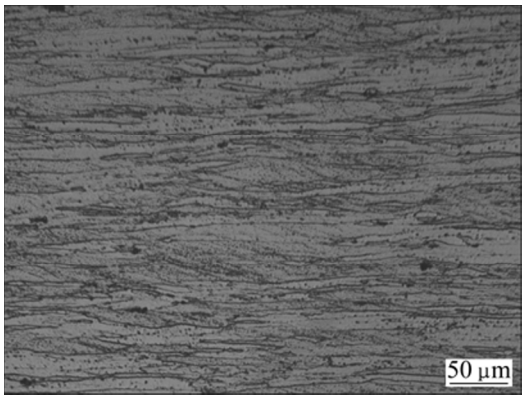

Fig. 10 Microstructure of as-solution treated alloy deformed at 350 °C and 1 s^{-1}

5 Conclusions

1) The efficiency of power dissipation of the as-solution treated alloy is higher than that of the as-homogenized alloy.

2) The domains of dynamic recrystallization for the as-homogenized and as-solution treated alloys occur at 400 °C, 0.01 s^{-1} and 450 °C, 0.001 s^{-1}, respectively.

3) The flow instability region of the as-solution treated alloy is wider than that of the as-homogenized alloy.

4) The precipitation characteristics are the main reason for the higher efficiency of power dissipation and the wider flow instability region of the as-solution treated alloy.

References

[1] HEINZ A, HASZLER A, KEIDEL C, MOLDENHAUER S, BENEDICTUS R, MILLER W S. Recent development in aluminium alloys for aerospace applications [J]. Materials Science and Engineering A, 2000, 280(1): 102−107.

[2] WARNER T. Recently-developed aluminum solutions for aerospace applications [J]. Material Science Forum, 2006, 519/521(2): 1271−1278.

[3] JIN N, ZHANG H, HAN Y, WU W X, CHEN J H. Hot deformation behavior of 7150 aluminum alloy during compression at elevated temperature [J]. Materials Characterization, 2009, 60(6): 530−536.

[4] ZHEN L, HU H, WANG X, ZHANG B, SHAO W. Distribution characterization of boundary misorientation angle of 7050 aluminum alloy after high-temperature compression [J]. Journal of Materials Processing Technology, 2009, 209(2): 754−761.

[5] HU H, ZHEN L, ZHANG B, YANG L, CHEN J Z. Microstructure characterization of 7050 aluminum alloy during dynamic recrystallization and dynamic recovery [J]. Materials Characterization, 2008, 59(9): 1185−1189.

[6] WANG Y, ZHANG Y, ZENG X, DING W. Characterization of dynamic recrystallisation in as-homogenized Mg−Zn−Y−Zr alloy using processing map [J]. Journal of Materials Science, 2006, 41(12): 3603−3608.

[7] ANBUSELVAN S, RAMANATHAN S. Hot deformation and processing maps of extruded ZE41A magnesium alloy [J]. Material and Design, 2010, 31(5): 2319−2233.

[8] SARKAR J, PRASAD Y, SURAPPA M. Optimization of hot workability of an Al−Mg−Si alloy using processing maps [J]. Journal of Materials Science, 1995, 30(11): 2843−2848.

[9] MENG G, LI B, LI H, HUANG H, NIE Z. Hot deformation and processing maps of an Al−5.7 wt.% Mg alloy with erbium [J]. Materials Science and Engineering A, 2009, 517(1−2): 132−137.

[10] QUAN G Z, KANG B S, KU T W, SONG W J. Identification for the optimal working parameters of Al−Zn−Mg−Cu alloy with the processing maps based on DMM [J]. The International Journal of Advanced Manufacturing Technology, 2011, 56(9): 1069−1078.

[11] LEE K W, BAN J S, LEE M G, KIM G H, CHO K Z. Processing map for the hot working of Ti−8Ta−3Nb [J]. Journal of Mechanical Science and Technology, 2008, 22(5): 931−936.

[12] LI A, HUANG L, MENG Q, GENG L, CUI X. Hot working of Ti−6Al−3Mo−2Zr−0.3Si alloy with lamellar [alpha]+[beta] starting structure using processing map [J]. Material and Design, 2009, 30(5):

1625−1631.

[13] PRASAD Y, GEGEL H, DORAIVELU S, MALAS J, MORGAN J, LARK K. Modeling of dynamic material behavior in hot deformation: Forging of Ti-6242 [J]. Metallurgical and Materials Transactions A, 1984, 15(10): 1883−1892.

[14] VENUGOPAL S, MANNAN S, PRASAD Y. Influence of cast versus wrought microstructure on the processing map for hot working of stainless steel type AISI 304 [J]. Materials Letters, 1993, 17(6): 388−392.

[15] VENUGOPAL S, SIVAPRASAD P, VASUDEVAN M, MANNAN S, JHA S, PANDEY P. Validation of processing maps for 304L stainless steel using hot forging, rolling and extrusion [J]. Journal of Materials Processing Technology, 1996, 59(4): 343−350.

[16] SIVAKESAVAM O, PRASAD Y. Hot deformation behaviour of as-cast Mg−2Zn−1Mn alloy in compression: A study with processing map [J]. Materials Science and Engineering A, 2003, 362(1): 118−124.

[17] ANBU S, RAMANATHAN S. Hot workability of as-cast and extruded ZE41A magnesium alloy using processing maps [J]. Transactions of Nonferrous Metals Society of China, 2011, 21(1): 257−264.

[18] RAVICHANDRAN N, PRASAD Y. Dynamic recrystallization during hot deformation of aluminum: A study using processing maps [J]. Metallurgical and Materials Transactions A, 1991, 22(10): 2339−2348.

[19] CHEN S Y, CHEN K H, PENG G S, JIA L, DONG P X. Effect of heat treatment on strength, exfoliation corrosion and electrochemical behavior of 7085 aluminum alloy [J]. Materials and Design, 2012, 35(3): 93−98.

[20] CHEN S Y, CHEN K H, PENG G S, CHEN X H, CENG Q H. Effect of heat treatment on hot deformation behavior and microstructure evolution of 7085 aluminum alloy [J]. Journal of Alloys and Compounds, 2012, 537(10): 338−345.

[21] CHEN S Y, CHEN K H, JIA L, PENG G S. Effect of hot deformation conditions on grain structure and properties of 7085 aluminum alloy [J]. Transactions of Nonferrous Metals Society of China, 2013, 23(2): 329−334.

[22] CERRI E, EVANGELISTA E, FORCELLESE A, McQUEEN H. Comparative hot workability of 7012 and 7075 alloys after different pretreatments [J]. Materials Science and Engineering A, 1995, 197(2): 181−198.

初始显微组织对 7085 铝合金热加工性能的影响

陈送义，陈康华，彭国胜，贾 乐

中南大学 粉末冶金国家重点实验室，长沙 410083

摘 要：采用等温压缩实验研究不同初始显微组织(均匀化态和固溶态)的 7085 铝合金在变形温度为 300~450 °C、应变速率为 0.0001~1 s^{-1} 热变形条件下的热加工性能。根据流变应力估算不同状态的合金应变速率敏感因子，并建立功率耗散图和失稳图。结果表明，均匀化态合金的有效功率消耗低于固溶态合金的有效功率消耗。均匀化态和固溶态合金的峰值动态再结晶变形参数分别为 400 °C、0.01 s^{-1} 和 450 °C、0.001 s^{-1}。均匀化态合金的流变不稳定区比固溶态合金的窄。两种初始组织的合金的热加工图的区别主要与合金的析出特征相关。

关键词：7085 铝合金；初始显微组织；热加工性；加工图；应变速率敏感因子

(Edited by Wei-ping CHEN)